



**HAL**  
open science

# pH-Dependent Changes in Structural Stabilities of Bt Cry1Ac Toxin and Contrasting Model Proteins following Adsorption on Montmorillonite

Wenqiang Zhao, Céline Poncet-Legrand, Siobhan Staunton, Hervé Quiquampoix

► **To cite this version:**

Wenqiang Zhao, Céline Poncet-Legrand, Siobhan Staunton, Hervé Quiquampoix. pH-Dependent Changes in Structural Stabilities of Bt Cry1Ac Toxin and Contrasting Model Proteins following Adsorption on Montmorillonite. *Environmental Science and Technology*, 2023, 57 (14), pp.5693-5702. 10.1021/acs.est.2c09310 . hal-04065678

**HAL Id: hal-04065678**

**<https://hal.science/hal-04065678>**

Submitted on 11 Jul 2023

**HAL** is a multi-disciplinary open access archive for the deposit and dissemination of scientific research documents, whether they are published or not. The documents may come from teaching and research institutions in France or abroad, or from public or private research centers.

L'archive ouverte pluridisciplinaire **HAL**, est destinée au dépôt et à la diffusion de documents scientifiques de niveau recherche, publiés ou non, émanant des établissements d'enseignement et de recherche français ou étrangers, des laboratoires publics ou privés.

This document is confidential and is proprietary to the American Chemical Society and its authors. Do not copy or disclose without written permission. If you have received this item in error, notify the sender and delete all copies.

**pH-dependent changes in structural stabilities of Bt Cry1Ac toxin and contrasting model proteins following adsorption on montmorillonite**

Journal:	<i>Environmental Science &amp; Technology</i>
Manuscript ID	es-2022-09310m.R1
Manuscript Type:	Article
Date Submitted by the Author:	n/a
Complete List of Authors:	Zhao, Wenqiang; Chinese Academy of Sciences, CAS Key Laboratory of Mountain Ecological Restoration and Bioresource Utilization & Ecological Restoration Poncet-Legrand, Celine; INRAE, SPO Staunton, Siobhan; INRAE, Eco&Sols Quiquampoix, Herve; INRAE, Eco&Sols

SCHOLARONE™  
Manuscripts

1  
2  
3  
4 1 **pH-dependent changes in structural stabilities of Bt Cry1Ac toxin and contrasting**  
5  
6 2 **model proteins following adsorption on montmorillonite**  
7

8  
9 3 Wenqiang Zhao<sup>a,b</sup>, Céline Poncet-Legrand<sup>c</sup>, Siobhán Staunton<sup>a,\*</sup>, Hervé Quiquampoix <sup>a,\*</sup>  
10

11  
12 4 <sup>a</sup>*Eco&Sols, INRAE, IRD, Cirad, Institut Agro, Univ Montpellier, Montpellier, France*  
13

14 5 <sup>b</sup>*CAS Key Laboratory of Mountain Ecological Restoration and Bioresource Utilization &*  
15  
16 6 *Ecological Restoration Biodiversity Conservation Key Laboratory of Sichuan Province,*  
17  
18 7 *Chengdu Institute of Biology, Chinese Academy of Sciences, Chengdu 610041, China*  
19  
20

21 8 <sup>c</sup>*SPO, Institut Agro, INRAE, Univ Montpellier, Montpellier, France.*  
22

23 9 \* Corresponding authors at:  
24

25  
26 10 *Eco&Sols, INRAE, IRD, Cirad, Institut Agro, Univ Montpellier, Montpellier, France.*  
27

28 11 *E-mail addresses:*  
29

30 12 *siobhan.staunton@inrae.fr; siobhan.staunton.inrae@gmail.com (S. Staunton)*  
31

32 13 *herve.quiquampoix@inrae.fr (H. Quiquampoix)*  
33  
34  
35  
36  
37  
38  
39  
40  
41  
42  
43  
44  
45  
46  
47  
48  
49  
50  
51  
52  
53  
54  
55  
56  
57  
58  
59  
60

1  
2  
3 14 **ABSTRACT**  
4

5 15 The environmental fate of insecticidal Cry proteins, including time-dependent conservation of  
6  
7 16 biological properties, results from their structural stability in soils. The complex cascade of  
8  
9 17 reactions involved in biological action requires Cry proteins to be in solution. However, the pH-  
10  
11 18 dependent changes in conformational stability and the adsorption-desorption mechanisms of  
12  
13 19 Cry protein on soil mineral remain unclear. We used DLVO calculation and differential  
14  
15 20 scanning calorimetry to interpret the driving forces and structural stabilities of Cry1Ac and two  
16  
17 21 contrasting model proteins adsorbed by montmorillonite. The structural stability of Cry1Ac is  
18  
19 22 closer to the “hard” protein,  $\alpha$ -chymotrypsin, relative to the “soft” bovine serum albumin (BSA).  
20  
21 23 The pH-dependent adsorption of Cry1Ac and  $\alpha$ -chymotrypsin could be explained by DLVO  
22  
23 24 theory, whereas the BSA adsorption deviated from it. Patch controlled electrostatic attraction,  
24  
25 25 hydrophobic effects and entropy changes following protein unfolding on mineral surface could  
26  
27 26 contribute to Cry1Ac adsorption. Cry1Ac, like chymotrypsin, was partly denatured on  
28  
29 27 montmorillonite and its structural stability decreased with increasing pH. Moreover, small  
30  
31 28 changes in conformational heterogeneity of both Cry1Ac and chymotrypsin were observed  
32  
33 29 following adsorption. Conversely, adsorbed BSA was completely denatured regardless of  
34  
35 30 solution pH. The moderate conformational rearrangement of adsorbed Cry1Ac may partially  
36  
37 31 explain why the insecticidal activity of Bt toxin appears to be conserved in soils, albeit for a  
38  
39 32 relatively short time period.  
40  
41  
42  
43  
44  
45  
46  
47

48 33 *Keywords:* Cry1Ac protein,  $\alpha$ -chymotrypsin, bovine serum albumin (BSA), adsorption,  
49  
50 34 structural stability, differential scanning calorimetry (DSC)  
51  
52  
53  
54  
55  
56  
57  
58  
59  
60

## 1. Introduction

Transgenic *Bacillus thuringiensis* (Bt) crops have been widely planted in the past two decades due to their benefits for agriculture <sup>1,2</sup>. Although their use is restricted in Europe, they account for a large proportion of some crops worldwide (e.g., 80% for cotton and 32% for maize), with almost 100% uptake rates for some countries <sup>3</sup>. Bt crops release insecticidal Cry proteins into agricultural soils through root exudates and decomposition of residues <sup>4,5</sup>. They are rapidly and somewhat irreversibly adsorbed on soil mineral surfaces, and this adsorption largely determines their environmental fate <sup>6-9</sup>. Soil is known to be an important long-term reservoir for another class of proteins of environmental concern, namely prions, which are responsible for spongiform encephalopathy diseases with a remanence of infectivity of several years <sup>10,11</sup>. In contrast to prion proteins, Cry proteins appear to lose their biological activity more rapidly, within days or weeks, following adsorption <sup>12-17</sup>. This has important implications for monitoring programs, the non-lethal exposure of target insects, and the possible exposure of non-target soil-dwelling organisms <sup>18-20</sup>.

Desorption of Cry protein from ingested soil and enzymatic cleavage within an insect mid-gut is the limiting factor for toxicity. The insecticidal properties of Cry proteins involve a complex cascade of reactions, and require the protein to be in solution <sup>21,22</sup>. The temperature effects on protein adsorption and persistence in soil have led to the hypothesis that the decline in toxicity is due to physicochemical processes, which cause conformational changes of the adsorbed protein and increase its fixation, rather than microbial breakdown <sup>15,16</sup>. Because of the importance of interfacial interaction in regulating Cry protein persistence and toxicity in soil, a few previous studies have tried to characterize the conformational stability of adsorbed Cry proteins on surfaces. For instance, Sander et al. <sup>6</sup> observed high conformational stability of Cry1Ab as demonstrated by the absence of any supply rate dependence of the extent of Cry1Ab adsorption on apolar gold-coated QCM-D sensors. Madliger et al. <sup>23</sup> reported that Cry1Ab

1  
2  
3 60 adsorption on and desorption from SiO<sub>2</sub> particles retained bioactivity, indicating high protein  
4  
5 61 conformational stability during adsorption-desorption cycles. Helassa et al.<sup>8</sup> monitored the  
6  
7 62 NH/ND exchange kinetics of Cry1Aa protein by FTIR spectroscopy and found that the  
8  
9 63 monomeric Cry1Aa toxin was adsorbed on montmorillonite without significant change of  
10  
11 64 secondary structure. However, the reported high structural stability of Cry toxin was based on  
12  
13 65 indirect evidences or partial quantification of molecular-level secondary structure (including  
14  
15 66 only  $\alpha$ -helix and  $\beta$ -sheets), which could not provide sufficient explanation for the rapid and  
16  
17 67 marked decline of insecticidal activity of soil-adsorbed Cry proteins within days or weeks<sup>12, 16,</sup>  
18  
19 68 <sup>17</sup>. To date, we still lack a macroscopic-level quantification of the overall structural stability of  
20  
21 69 adsorbed Cry protein, which may be useful for the better interpretation of its relatively short-  
22  
23 70 term persistence and decreased bioactivity in soil environment. The conformational changes of  
24  
25 71 various model proteins adsorbed by different surfaces have been widely reported<sup>24-28</sup>. Both the  
26  
27 72 extent of adsorption and the resulting conformation changes are strongly dependent on pH<sup>7, 29,</sup>  
28  
29 73 <sup>30</sup>. However, we are unaware of any research that has examined the pH-dependent structural  
30  
31 74 changes of Cry protein regulated by adsorption.  
32  
33  
34  
35  
36

37  
38 75 Differential scanning calorimetry (DSC) provides a sensitive probe for protein-surface  
39  
40 76 interaction<sup>31</sup>, which has been used in this work for the first time to compare the structural  
41  
42 77 stability of free and surface bound Cry proteins. The information gained from DSC is on a  
43  
44 78 macroscopic level, which enables the evaluation of the overall protein conformation<sup>32</sup>. Valid  
45  
46 79 parameters on protein stability and structural heterogeneity can be obtained from the  
47  
48 80 thermogram of protein unfolding process with increasing temperature, which are characterized  
49  
50 81 in terms of enthalpy, denaturation temperature, and the width of transition<sup>33</sup>. A few studies  
51  
52 82 have discussed the possible forces contributing to Cry protein adsorption on SiO<sub>2</sub> and humic  
53  
54 83 substances<sup>6, 34-36</sup>. However, their conclusions were based on the indirect observations of the  
55  
56 84 different adsorption or desorption phenomena of Cry proteins on several surfaces varying in  
57  
58  
59  
60

1  
2  
3 85 polarity and charge. Predictive models of protein-surface interactions, including the classical  
4  
5 86 Derjaguin-Landau-Verwey-Overbeek (DLVO) theory, may also be of use<sup>37-39</sup> To date, the pH-  
6  
7 87 dependent DLVO interaction energies of surface-bound Cry toxin have not been quantitatively  
8  
9 88 interpreted. The comparison of DLVO prediction with experimental adsorption capacity may  
10  
11 89 be an effective method to evaluate if non-DLVO interactions contribute to structural  
12  
13 90 rearrangements in adsorbed proteins.

14  
15  
16  
17 91 The objectives of this work were to elucidate directly the adsorption-induced changes of  
18  
19 92 structural stabilities of Cry protein adsorption on a representative soil clay mineral  
20  
21 93 (montmorillonite) at various pH, and to deduce the driving forces using DSC, physico-chemical  
22  
23 94 characterization techniques and DLVO theory. Two well-studied model proteins, bovine serum  
24  
25 95 albumin (BSA) and  $\alpha$ -chymotrypsin, were used as reference proteins to compare with the  
26  
27 96 conformational flexibility of a Cry toxin. BSA has a large conformational adaptability (“soft”  
28  
29 97 protein), while chymotrypsin exhibits a much stronger internal coherence (“hard” protein)<sup>40</sup>.  
30  
31 98 <sup>41</sup>. Montmorillonite was chosen as a model mineral because of its large adsorption capacity for  
32  
33 99 Bt proteins in comparison to other soil minerals (for example goethite, kaolinite, hematite,  
34  
35 100 gibbsite and silica)<sup>7, 42, 43</sup>, and its negative pH-independent surface charge that facilitates the  
36  
37 101 investigation of pH-dependent adsorption phenomena<sup>8</sup>.

## 102 **2. Materials and methods**

### 103 *2.1. Sample preparation*

104 A natural strain of *Bacillus thuringiensis* subsp. Kurstaki HD73 that produces Cry1Ac  
105 protein was used. Cry1Ac toxin was chosen because of its expression in an important Bt crop  
106 (cotton) around the world<sup>44</sup>. This bacterial strain was cultivated in a fermentor, and activated  
107 and purified as described previously<sup>7</sup>. Due to the small concentrations of Cry proteins detected  
108 in soils (0.1 to 100 ng of toxin g<sup>-1</sup>)<sup>45,46</sup>, the protein would probably be present as monomers<sup>47</sup>.  
109 A pH above 6.5 and an ionic strength (IS) of at least 150 mM NaCl were necessary to keep the

1  
2  
3 110 protein in a monomeric state <sup>7</sup>. To prevent polymerization, the purified toxin was stored in 10  
4  
5 111 mM CAPS (3-(Cyclohexylamino)-1-propanesulfonic acid), 350 mM NaCl, and pH 10.4 at -20  
6  
7 112 °C before use <sup>8</sup>. When required, the protein was slowly defrosted at 4 °C, and then the electrolyte  
8  
9 113 solution was exchanged by repeated centrifugation in an Amicon tube followed by dilution in  
10  
11 114 10 mM MOPS solution (3-(N-morpholino)propanesulfonic acid) containing 150 mM NaCl (pH  
12  
13 7.0, 8.0 or 9.0). The monomeric Cry1Ac has a molecular weight of 67 kDa and an isoelectric  
14  
15 115 point (IEP) of 6.4.  
16  
17 116

18  
19 117 Alpha-chymotrypsin (C4129, type II, from bovine pancreas) and bovine serum albumin  
20  
21 118 (BSA, CAS No. 9048-46-8) were both purchased from Sigma-Aldrich, and were used without  
22  
23 119 further treatment. The molecular dimension of chymotrypsin is  $5 \times 6 \times 6$  nm<sup>3</sup>. It consists of 3  
24  
25 120 polypeptide chains bound by 2 inter strands disulfide bridges. Its IEP and molecular weight are  
26  
27 121 8.1 and 25 kDa, respectively <sup>48</sup>. Chymotrypsin was dissolved in buffer solution of 10 mM  
28  
29 122 NaH<sub>2</sub>PO<sub>4</sub> at pH 7.0, 8.0 or 9.0.  
30  
31 123

32  
33 124 BSA is a globular, heart shaped ( $8 \times 3 \times 3$  nm), flexible protein with an IEP of 4.8 and  
34  
35 125 molecular weight of 66.4 kDa. It is composed of 100 acidic and 99 basic side acids <sup>49</sup>. BSA was  
36  
37 126 dissolved in 10 mM NaH<sub>2</sub>PO<sub>4</sub> and 10 mM CH<sub>3</sub>COONa solution (pH 4.0, 4.6 or 5.2) for  
38  
39 127 subsequent experiments. The above buffer solutions have been used in previous studies <sup>6-8, 36,</sup>  
40  
41 128 <sup>50-52</sup> to ensure that these proteins were always in monomeric forms and carried different net  
42  
43 129 surface charges at pH values above or below their IEPs (shown in Fig. 1) for the comprehensive  
44  
45 130 comparison of their structural stabilities.  
46  
47 131

48  
49 132 The clay mineral used was SWy-1 Wyoming montmorillonite obtained from the Source  
50  
51 133 Clays Repository of the Clay Minerals Society (Columbia, MO) <sup>53</sup>. The clay-sized fraction (<2  
52  
53 134 μm) was obtained by sedimentation and then saturated in sodium by repeated washings in 1 M  
54  
55 NaCl followed by washing in water and dialysis to provide a salt-free suspension, as previously  
56  
57 described <sup>7</sup>. The specific surface area of this montmorillonite is 800 m<sup>2</sup> g<sup>-1</sup> <sup>54, 55</sup>. The surface is  
58  
59  
60

1  
2  
3 135 negatively charged over the tested pH range. All solutions were prepared using deionised water  
4  
5 136 from a Milli-Q purification system.  
6  
7

## 8 9 137 *2.2. Characterization of proteins and mineral*

10  
11 138 The hydrodynamic diameters and electrophoretic mobilities of proteins and  
12  
13 139 montmorillonite were determined using a Zetasizer (Nano ZS, Malvern Instruments Ltd., UK).

14  
15 140 Size distribution (% number) was measured by dynamic light scattering (DLS) and analyzed  
16  
17  
18 141 by the Malvern software. The light scattered by the sample was measured at a backscatter angle  
19  
20 142 of 173° and the correlation functions were analyzed with a non-linear least squares fit. All DLS  
21  
22 143 measurements were conducted at 20 °C and repeated three times at different IS and pH values  
23  
24 144 (Table S1), and the experiment concentrations for Cry1Ac, chymotrypsin and BSA were 0.4,  
25  
26 145 0.5 and 0.5 mg mL<sup>-1</sup>, respectively.  
27  
28

29 146 The zeta potential was then calculated from the electrophoretic mobility using the  
30  
31 147 Smoluchowski equation. Solution pH values were chosen to encompass the IEP of each protein.  
32  
33 148 Thus different net surface charges of proteins could be observed and discussed in this study.  
34  
35

36 149 Hydrophobicity analysis was conducted by the adhesion to hydrocarbon test<sup>56, 57</sup>. Briefly,  
37  
38 150 1 mL of *n*-dodecane (laboratory grade) was added to 4 mL of protein solution or mineral  
39  
40 151 suspension (OD<sub>initial</sub>) in 10 mL test tube. The mixture was vortexed at full speed for 2 min,  
41  
42 152 followed by a 45 min rest period to obtain phase separation. The aqueous phase was pipetted  
43  
44 153 into another tube and its optical density (OD<sub>final</sub>) was determined by uv-visible  
45  
46 154 spectrophotometry. The hydrophobicity (%) was quantified as the percent of total proteins or  
47  
48 155 montmorillonite partitioned into the hydrocarbon phase: hydrophobicity = [(OD<sub>initial</sub> - OD<sub>final</sub>)  
49  
50 156 / OD<sub>initial</sub>] × 100. The mean percentage of hydrophobicity was calculated using duplicate or  
51  
52 157 triplicate samples across a range of IS and pH values.  
53  
54  
55  
56  
57

## 58 158 *2.3. Adsorption measurement*

59  
60

1  
2  
3 159 The prepared protein solutions (methods shown in 2.1. *Sample preparation*) were mixed  
4  
5 160 with 2 mg of montmorillonite to reach a final volume of 2 mL. Protein-mineral mixtures were  
6  
7 161 statically incubated at 20 °C for 1 h to minimize protein denaturation at the water-air interface  
8  
9  
10 162 <sup>58</sup>. Preliminary experiments showed that 1 h was sufficient for the reactions to reach an  
11  
12 163 equilibrium. After incubation, phases were separated by centrifugation at 20000 × g for 30 min.  
13  
14 164 The concentration of non-adsorbed protein (mg mL<sup>-1</sup>) in the supernatant solution as well as the  
15  
16 165 calibration curve were quantified by uv-visible spectrophotometry (Cry1Ac – wavelength 280  
17  
18 166 nm; chymotrypsin – 280 nm; BSA – 279 nm). Control experiments were performed in the  
19  
20 167 absence of proteins. The amount of adsorbed protein was calculated from the difference in  
21  
22 168 concentration before and after centrifugation, and the adsorption percentage (%) of protein was  
23  
24 169 also calculated. The experimental conditions of adsorption tests for each protein (Cry1Ac,  
25  
26 170 chymotrypsin and BSA) are indicated in Table S1. The adsorption of each protein with a fixed  
27  
28 171 initial concentration was measured at 3 different pH values. These conditions were chosen to  
29  
30 172 ensure that sufficient amounts of protein were adsorbed on montmorillonite, and that the  
31  
32 173 proteins were always monomers (determined by dynamic light scattering). *Previous studies*  
33  
34 174 *used comparable solution conditions* (protein concentration of 0.02–1.6 mg mL<sup>-1</sup>; pH 3–8; ionic  
35  
36 175 strength of 3–50 mM) to avoid protein-protein interactions that may result in bi- to multilayer  
37  
38 176 adsorption <sup>6, 36, 50-52</sup>. All adsorption experiments were performed in triplicate. Statistical  
39  
40 177 differences among adsorption or characterization data were analyzed using a Student's t test in  
41  
42 178 SPSS 17.0 software (SPSS Inc., Chicago, USA).

#### 43 179 *2.4. Calculation of protein-mineral DLVO interaction energy*

44 180 The DLVO theory was used to explain the adsorption of protein on solid surfaces as a  
45 181 function of separation distance by calculating the interaction energies between colloidal  
46 182 particles <sup>59</sup>. Total interaction energies were quantified as the sum of van der Waals and  
47 183 electrostatic interactions, which were calculated from the particle-substrate <sup>21</sup> potentials based

1  
2  
3 184 on the DLVO theory <sup>60, 61</sup>. Positive interaction energy represents a repulsive force, while  
4  
5 185 negative energy indicates an attraction <sup>62</sup>. Further details on the calculation of electrostatic  
6  
7 186 interaction energy ( $\Phi_{EDL}$ ) <sup>63, 64</sup> and van der Waals attractive interaction energy ( $\Phi_{VDW}$ ) <sup>63, 65</sup> are  
8  
9  
10 187 provided in the Supporting Information.

### 13 188 *2.5. Differential scanning calorimetry*

15 189 DSC experiments were carried out using a microcalorimeter (VP DSC, MicroCal Inc.,  
16  
17  
18 190 Northampton, MA) to measure the excess heat capacity ( $C_p$ , kcal/mol/°C) of protein as a  
19  
20 191 function of temperature <sup>33</sup>. The same procedure and buffer solution for adsorption measurement  
21  
22 192 were used to prepare individual protein suspensions and protein-mineral mixtures for DSC  
23  
24 193 analysis. Proteins were mixed with various buffers or montmorillonite and gently injected into  
25  
26 194 the sample-ampoule (0.5 mL) via a syringe. Corresponding buffers or montmorillonite  
27  
28 195 suspensions were used as references. The ampoules were allowed to stabilize at 20 °C for 10  
29  
30 196 min prior to the up-scanning experiment. Up-scan and down-scan rates of 60 °C/h were used  
31  
32 197 <sup>66</sup>. Released  $C_p$  value of the sample-ampoule was recorded relative to the reference ampoule in  
33  
34 198 the temperature range of 20–85 °C. Protein concentrations used in this study (0.4–0.5 mg mL<sup>-1</sup>)  
35  
36 199 <sup>1</sup>) generated satisfactory transition signals during the DSC measurements, and avoided  
37  
38 200 aggregation phenomena of proteins. The montmorillonite particles showed negligible  
39  
40 201 endothermic or exothermic transitions over the temperature range examined.

45 202 To obtain the heat capacity derived from the adsorbed protein, the heat capacity of the  
46  
47 203 mineral particles in the buffer and supernatant protein in adsorption mixture (after  
48  
49 204 centrifugation) were measured and subtracted from the protein-mineral adsorption mixture  
50  
51 205 measurement <sup>67</sup>. The DSC curves of free and adsorbed proteins were corrected for the baselines  
52  
53 206 by subtracting reference scan, and then analyzed with MicroCal Origin 7.0 software <sup>31</sup>. The  
54  
55 207 transition process of protein was recognized as a sharp endothermic peak. The denaturation  
56  
57 208 temperature  $T_m$  (°C) is defined as the temperature at which the maximum  $C_p$  occurs <sup>24</sup>. The  
58  
59

1  
2  
3 209 calorimetric enthalpy ( $\Delta H$ , kcal/mol) is calculated from the area of the transition peak, which  
4  
5 210 is correlated with the content of ordered secondary structure in protein. The sharpness of the  
6  
7 211 transition peak can be measured as the full width of transition at half maximum of the transition  
8  
9 212 peak (FWHM, °C). It is an index of the cooperative nature of the transition from native to  
10  
11 213 denatured state <sup>67</sup>.

### 15 214 **3. Results and discussion**

#### 17 215 *3.1. Protein and mineral properties*

19 216 Zeta potential reflects the net charge on colloidal surface. Fig. 1 shows that the zeta  
20  
21 217 potentials of Cry1Ac (from -8.8 mV to -15.1 mV) and BSA (from 16.9 mV to -3.1 mV)  
22  
23 218 became more negative with increased pH, which was ascribed to the deprotonation of functional  
24  
25 219 groups with the addition of base <sup>68</sup>. Chymotrypsin possessed a small amount of surface charge  
26  
27 220 (from 0.4 mV to -3.6 mV). Montmorillonite was the most negatively charged, and the zeta  
28  
29 221 potential values were significantly higher at IS of 10 mM MOPS+150 mM NaCl (from -38.8  
30  
31 222 mV to -43.8 mV) than those at low IS of 10 mM (from -48.9 mV to -55.1 mV) ( $P < 0.05$ ).  
32  
33 223 This result was attributed to the charge screening by counter ions and double layer compression  
34  
35 224 outside the mineral surfaces <sup>34</sup>.

36 225 The hydrodynamic diameters of Cry1Ac (~8 nm), chymotrypsin (~6 nm), BSA (~10 nm)  
37  
38 226 as well as their size distributions confirmed that proteins were all in monomeric states under  
39  
40 227 the tested conditions (Table S2 and Fig. S1). These values were comparable to the data reported  
41  
42 228 by previous literature <sup>69-71</sup>. [Different extents of electrostatic energies and self-associations](#)  
43  
44 229 [among protein molecules as well as interactions between protein and buffer molecules could](#)  
45  
46 230 [occur at various pH, and thus affect the hydrodynamic diameters of proteins and diffusion](#)  
47  
48 231 [coefficients](#) <sup>70,71</sup>. Montmorillonite showed a bimodal particle size distribution at low pH of 4.0–  
49  
50 232 [5.2](#). The sizes of montmorillonite platelets (>60 nm) were much larger than those of proteins  
51  
52 233 (<12 nm) ( $P < 0.05$ ). Generally, the size distribution of each protein showed insignificant

234 variation with pH ( $P > 0.05$ ).

235 The hydrophobicities (%) of proteins and montmorillonite are presented in Table S3. Across  
236 the solution conditions tested, chymotrypsin (42.9%–50.2%) and BSA (21.7%–40.1%) were  
237 relatively more hydrophobic than Cry1Ac (9.3%–11.3%) and montmorillonite (3.0%–13.3%)  
238 ( $P < 0.05$ ). The hydrophobicities of BSA showed large difference at varied pH ( $P < 0.05$ ), while  
239 those of other proteins and montmorillonite were generally consistent over different pH values  
240 ( $P > 0.05$ ).

### 241 3.2. Protein adsorption on montmorillonite

242 As shown in Fig. S2, the adsorption percentages followed the sequence of: BSA (99.5%–  
243 99.7%) > Cry1Ac (78.9%–87.2%) > chymotrypsin (62.1%–68.6%). BSA had the lowest energy  
244 barrier ( $0.19 k_B T$ ), which yielded the weakest repulsive interaction and improved its adsorption  
245 on montmorillonite (Table 1). This trend was consistent with the DLVO theory and  
246 demonstrated that van der Waals and electrostatic forces played a significant role in protein  
247 adsorption<sup>72</sup>. The energy barriers of Cry1Ac ( $0.14$ – $1.11 k_B T$ ) were stronger than those of  
248 chymotrypsin ( $< 0.52 k_B T$ ), revealing the stronger repulsive interactions between Cry1Ac and  
249 mineral. However, the percentages of Cry1Ac adsorbed were found to be larger than  
250 chymotrypsin. Several mechanisms might be involved in the Cry1Ac adsorption process to  
251 provide additional adsorption energy. Firstly, previous work confirmed that a similar Cry  
252 protein (Cry1Ab) had nonuniform surface charge distribution because domain II (IEP of 9.4)  
253 and III (IEP of 9.6) carried positive charges below pH 9, suggesting the patch controlled  
254 electrostatic attraction (PCEA) determined Cry1Ab adsorption on SiO<sub>2</sub><sup>23,34</sup>. In this study, the  
255 Cry1Ac molecules (88% identical sequence to Cry1Ab) tended to be oriented with positive  
256 patches towards montmorillonite especially at high IS<sup>36,73</sup>, which caused greater adsorption  
257 than that predicted by electrostatic energy. Secondly, after Cry1Ac adsorption on the mineral  
258 surface at pH 7.0–9.0, its losses of  $\Delta H$  percentages (62.5%–67.5%) were slightly greater than

1  
2  
3 259 the “hard” protein – chymotrypsin (55.1%–61.6%) (Tables 2 and 3). Hence, the contribution of  
4  
5 260 entropy resulted from the greater unfolding processes of adsorbed Cry1Ac was likely to  
6  
7 261 enhance its adsorption phenomenon <sup>67</sup>. Finally, the hydrophobic residues at the protein surface  
8  
9 262 can play a crucial role in adsorption when both surface and protein are negatively charged <sup>72</sup>. It  
10  
11 263 has been reported that the interactions between the residues of  $\alpha 7$  helix and the residues of  $\alpha 6$   
12  
13 264 helix together constitute a hydrophobic network in Cry1Ac protein <sup>74</sup>, and the hydrophobic  
14  
15 265 residues also exist in the loop regions of Cry1Ac domain II <sup>75</sup>. The above hydrophobic residues  
16  
17 266 were closely related to the correct folding of the molecule and the toxin-inclusion formation,  
18  
19 267 which would affect Cry protein stability and adsorption on surfaces <sup>8, 74</sup>. The montmorillonite  
20  
21 268 surface also exhibits some degree of hydrophobicity (Table S3). Thus, the hydrophobic effect  
22  
23 269 could contribute to Cry1Ac adsorption on the relatively apolar siloxane surface of  
24  
25 270 montmorillonite. Overall, the main driving forces of Cry1Ac adsorption were DLVO forces,  
26  
27 271 PCEA, and hydrophobic interaction as well as the configurational entropy gained upon the  
28  
29 272 structural rearrangements in proteins.  
30  
31  
32  
33  
34

35 273 The adsorption of Cry1Ac and chymotrypsin on the mineral generally decreased with the  
36  
37 274 increase of solution pH ( $P < 0.05$ ). This trend was in agreement with the electrostatic and total  
38  
39 275 DLVO energies shown in Figs. 2a and 2b. High pH values generated larger electrostatic/DLVO  
40  
41 276 repulsions or lower attractions. In contrast, although the electrostatic and DLVO energies of  
42  
43 277 BSA-montmorillonite system revealed large changes with increasing pH (from attraction to  
44  
45 278 repulsion), the BSA molecules were almost completely adsorbed by montmorillonite regardless  
46  
47 279 of pH and differences in adsorption were not significant ( $P > 0.05$ ). This unexpected result  
48  
49 280 suggested that BSA adsorption phenomenon at different pH partially deviated from DLVO  
50  
51 281 theory, and other non-DLVO mechanisms may be involved. As unfolding of BSA on  
52  
53 282 montmorillonite has been shown by various methods <sup>49, 76</sup>, a loss of conformational entropy is  
54  
55 283 probably the secondary process responsible for the loss of the Gibbs energy of the system and  
56  
57  
58  
59  
60

1  
2  
3 284 its adsorption behavior <sup>40</sup>.

4  
5  
6 285 *3.3. DSC thermograms and thermodynamic parameters of proteins*

7  
8 286 The DSC thermogram for Cry1Ac or chymotrypsin showed a single endothermic peak at  
9  
10 287 varied pH (Figs. 3a and 3b), whereas transition peaks with shoulders at the left and right sides  
11  
12 288 were visible for BSA in Fig. 3c. A previous study also observed two transition peaks for BSA  
13  
14 289 adsorption on nanomaterials <sup>77</sup>. It suggested that the denaturation process did not follow a  
15  
16 290 simple two-state transition. The BSA molecule is folded into three domains in the native state,  
17  
18 291 and these domains may unfold at different temperature ranges <sup>78</sup>. The shapes and heights of the  
19  
20 292 transition peaks changed with the solution pH as well as the protein states (free or adsorbed),  
21  
22 293 indicating that the conformations of proteins were disturbed and some of the secondary  
23  
24 294 structures were unfolded after protein adsorption on montmorillonite.

25  
26 295 The DSC thermograms were evaluated with respect to the parameters of  $T_m$ ,  $\Delta H$ , and  
27  
28 296 FWHM. As seen in Table 2, compared to free Cry1Ac, the decrease in  $T_m$  (1.1–3.3 °C) and  
29  
30 297 reduction in  $\Delta H$  values (236.0–330.9 kcal/mol) for adsorbed Cry1Ac were found at pH 7.0–9.0.  
31  
32 298 It suggested that the surface bound-state Cry1Ac was partially denatured, and adsorbed Cry1Ac  
33  
34 299 was obviously less stable and structured than free Cry1Ac. As indicated by FWHM values, the  
35  
36 300 denaturation peaks for the adsorbed proteins were broader than for the free ones. This was an  
37  
38 301 indication of a weakened cooperativity in the melting process and a larger conformational  
39  
40 302 heterogeneity in the adsorbed state <sup>79</sup>. Our previous study observed that Cry1Aa adsorption on  
41  
42 303 montmorillonite had no effect on the  $\beta$ -sheets, but the  $\alpha$ -helical component decreased from 42%  
43  
44 304 to 38% after contact with the clay in the presence of 10 mM CAPS and 350 mM NaCl buffer <sup>8</sup>.  
45  
46 305 In the vicinity of the electronegative clay, the local higher concentration of counter ions could  
47  
48 306 protect the  $\alpha$ -helical domain from change <sup>8</sup>. Since Cry1Aa and Cry1Ac share a similar three-  
49  
50 307 dimensional structure consisting of three domains <sup>80, 81</sup>, it is reasonable to expect that the  
51  
52 308 relatively lower buffer concentration in this study (10 mM MOPS and 150 mM NaCl) may  
53  
54  
55  
56  
57  
58  
59  
60

1  
2  
3 309 induce greater extent of unfolding of the  $\alpha$ -helices in adsorbed Cry1Ac and lead to a reduction  
4  
5 310 in  $\Delta H$  value. In addition, the  $T_m$  and  $\Delta H$  values of free and adsorbed Cry1Ac decreased with  
6  
7 311 the increase of pH, suggesting lower Cry1Ac structural stability at higher pH. Cry1Ac was more  
8  
9 312 negatively charged at higher pH, and the electrostatic repulsions between Cry1Ac and mineral  
10  
11 313 became stronger, causing fewer Cry1Ac molecules to be adsorbed on montmorillonite with  
12  
13 314 lower surface coverage of proteins. Considering kinetic dynamics, the rate of Cry1Ac  
14  
15 315 molecules arriving at the mineral surface would be slower under these conditions, and therefore  
16  
17 316 the molecules would have more time and enough space to adjust their structure to the new  
18  
19 317 environment before a neighboring site became occupied by subsequently arriving molecules <sup>78</sup>.  
20  
21  
22  
23 318 <sup>82</sup>. Hence, Cry1Ac structural rearrangement was more pronounced under unfavorable  
24  
25 319 adsorption conditions, which probably modified its biological properties. This finding also  
26  
27 320 provides a coherent explanation for the more rapid decline in immunologically detectable Bt  
28  
29 321 toxin in sandy soils (lower surface coverage of protein) than clay textured soils reported by a  
30  
31 322 previous study <sup>15</sup>.

32  
33  
34  
35 323 Chymotrypsin is classified as a structurally “hard” protein <sup>41,83</sup>, and it is expected to undergo  
36  
37 324 little structural change upon adsorption. However, we found markedly lower structural stability  
38  
39 325 of adsorbed chymotrypsin in comparison to the free state (i.e.,  $\Delta H$  values decreased by 55.1%–  
40  
41 326 61.6%) (Table 3). It has been reported that a reduction in transition enthalpy, upon adsorption  
42  
43 327 onto silica particles, was observed for rigid proteins – lysozyme and RNase only at low IS (10  
44  
45 328 mM sodium) <sup>84</sup>. On the one hand, this result was ascribed to the low IS of the buffer solution  
46  
47 329 (10 mM NaH<sub>2</sub>PO<sub>4</sub>). At low IS the intramolecular electrostatic repulsion will dominate, leading  
48  
49 330 to the proteins being less rigid and thus enhancing their ability to alter steric conformation <sup>85</sup>.  
50  
51 331 On the other hand, when unexpectedly large amounts (>25%) of chymotrypsin molecules were  
52  
53 332 adsorbed, hydrophobic interaction was involved in protein binding and chymotrypsin could  
54  
55 333 undergo extensive denaturation with loss of both tertiary and secondary structure <sup>56</sup>. Using  
56  
57  
58  
59  
60

1  
2  
3 334 molecular dynamics simulations, a previous study reported that the presence of negative  
4  
5 335 (aspartic acid) and hydrophobic (leucine) residues could contribute to the stable adsorption of  
6  
7 336 chymotrypsin on amorphous silica <sup>51</sup>. FTIR data in our previous work further showed that a  
8  
9  
10 337 small secondary structure unfolding affected about 15-20 peptide units of chymotrypsin after  
11  
12 338 its adsorption on montmorillonite <sup>83</sup>. With the partial loss of secondary structure, the unfolding  
13  
14 339 process of adsorbed chymotrypsin required smaller enthalpy than free protein. It should be also  
15  
16  
17 340 noted that the  $T_m$  values of adsorbed chymotrypsin were larger than those of free ones,  
18  
19 341 suggesting that the transition temperatures of chymotrypsin were delayed upon adsorption on  
20  
21 342 mineral surface. Considering the crowding of chymotrypsin molecules at the mineral surface,  
22  
23 343 intermolecular association among adsorbed chymotrypsin molecules probably existed on  
24  
25 344 montmorillonite particles during the DSC heating process. This surface aggregation could give  
26  
27 345 more thermal stability to the adsorbed chymotrypsin than the free protein, resulting in higher  
28  
29 346 transition temperatures <sup>86</sup>. The wider FWHM of transition peaks at higher pH also displayed  
30  
31 347 larger conformational heterogeneity of the adsorbed chymotrypsin, due to the uneven structural  
32  
33 348 changes of chymotrypsin molecules.

37 349 The  $T_m$  and  $\Delta H$  for free BSA in buffer solutions corresponded well with the values ( $T_m$ :  
38  
39 350 52.5–67.5 °C;  $\Delta H$ : 130.9–173.7 kcal/mol) reported elsewhere (Table 4) <sup>24, 67, 78</sup>. The  $\Delta H_1$  and  
40  
41 351  $\Delta H_2$  values for free BSA were the largest at pH 4.6, which was close to the IEP of BSA (4.8).  
42  
43 352 Under these conditions, the repulsive electrostatic energy (Fig. 2a) between the BSA molecules  
44  
45 353 was small, which caused weak intermolecular association (indicated by slightly larger  
46  
47 354 hydrodynamic diameter at pH 4.6, Table S2) and subsequent higher unfolding enthalpy. The  
48  
49 355 thermograms of adsorbed-state BSA showed negligible calorimetric signals, and the  
50  
51 356 denaturation enthalpies for adsorbed BSA were strongly reduced relative to those in solutions.  
52  
53 357 This result indicated that the adsorbed BSA was almost completely denatured, and the contents  
54  
55 358 of ordered secondary structure components ( $\alpha$ -helix and  $\beta$ -sheet) decreased markedly following  
56  
57  
58  
59  
60

1  
2  
3 359 adsorption<sup>49</sup>. In this work, since the BSA adsorption capacity was not mainly governed by  
4  
5 360 DLVO theory, the large decrease in BSA structural stability and the entropy gain originated  
6  
7 361 from the rearrangements within “soft” BSA molecule were the major reasons for the highest  
8  
9 362 BSA adsorption capacity<sup>67, 77</sup>. Hydrophobic interactions may also occur between the  
10  
11 363 hydrophobic subdomain IIIB of BSA and montmorillonite<sup>72</sup>.  
12  
13  
14

#### 15 364 3.4. Comparing the structural stability of Cry1Ac with model proteins

16  
17  
18 365 The extent of structural change for the adsorbed Cry1Ac on mineral was closer to  
19  
20 366 chymotrypsin than to BSA due to the following reasons: (i) the  $\Delta H$  values declined by 62.5%–  
21  
22 367 67.5% after the free Cry1Ac adsorbed on montmorillonite, which were comparable to the  
23  
24 368 percentage  $\Delta H$  decrease of chymotrypsin (55.1%–61.6%); (ii) Cry1Ac and chymotrypsin both  
25  
26 369 showed small changes of FWHM values (<0.5 °C) following adsorption on the mineral; and  
27  
28 370 (iii) the pH-dependent adsorption abilities of Cry1Ac or chymotrypsin were consistent with the  
29  
30 371 patterns predicted by DLVO theory, which may result from similar adsorption mechanisms as  
31  
32 372 well as comparable degrees of structural changes upon adsorption. In summary, Cry1Ac and  
33  
34 373 chymotrypsin were both partially denatured in the adsorbed state and their adsorption processes  
35  
36 374 could be explained by DLVO theory. In contrast, the “soft” BSA was unfolded to a great extent  
37  
38 375 and was totally denatured at the mineral-solution interface, while its pH-dependent adsorption  
39  
40 376 deviated from DLVO prediction.  
41  
42  
43  
44

45 377 The modelling of protein adsorption on solid surfaces dates back to the 1980s. Arai and  
46  
47 378 Norde<sup>87</sup> studied the principles governing adsorption by adapting existing theories for polymers  
48  
49 379 and taking into account the electrostatic interactions and the three-dimensional structures of  
50  
51 380 proteins. Norde and co-workers<sup>88</sup> deduced from their experimental data that the adsorption of  
52  
53 381 a protein is related to the stability of its native structure. Hard proteins have since been described  
54  
55 382 as having a higher unfolding energy than soft proteins (e.g., 60 kJ mol<sup>-1</sup> for the hard lysozyme  
56  
57 383 and 21 kJ mol<sup>-1</sup> for the soft  $\alpha$ -lactalbumin), and both proteins have a similar molecular weight  
58  
59  
60

1  
2  
3 384 <sup>89</sup>. In parallel, the energy required to unfold an  $\alpha$ -helix is lower than that required for a  $\beta$ -sheet,  
4  
5 385 and soft proteins are characterized by a higher  $\alpha$ -helix/ $\beta$ -sheet ratio than hard proteins <sup>9, 90</sup>. As  
6  
7 386 indicated by the changes of  $\Delta H$  values, the structural loss of adsorbed Cry1Ac was slightly  
8  
9 387 higher than chymotrypsin (hard protein) but much lower than BSA (soft protein). It is therefore  
10  
11 388 expected that the proteins in our study would have the following structures: 1) majority of  $\beta$ -  
12  
13 389 strands for chymotrypsin and fewer for Cry1 Ac; and 2) majority of  $\alpha$ -helices for BSA and  
14  
15 390 fewer for Cry1Ac. The Uniprot database allowed us to calculate the following proportions: BSA:  
16  
17 391 71%  $\alpha$ -helix, 3%  $\beta$ -strand (ratio 24);  $\alpha$ -chymotrypsin: 15%  $\alpha$ -helix, 43%  $\beta$ -strand (ratio 0.35);  
18  
19 392 Cry1 Ac: 28%  $\alpha$ -helix, 29%  $\beta$ -strand (ratio 1) <sup>91-93</sup>. The Cry1 protein has an intermediate  
20  
21 393 behavior between the two model proteins studied.  
22  
23  
24  
25  
26

#### 27 394 **4. Conclusions and environmental implications**

28  
29 395 To conclude, this is the first study to evaluate quantitatively the pH-dependent DLVO  
30  
31 396 theory driving Cry protein-clay mineral interaction, as well as the different structural stabilities  
32  
33 397 between Cry toxin and model proteins. A combination of electrostatic and van der Waals forces,  
34  
35 398 PCEA, hydrophobic effect and entropy gained from the protein unfolding process could  
36  
37 399 contribute to Cry1Ac adsorption on montmorillonite. The structural stability of Cry1Ac protein  
38  
39 400 was slightly lower than the “hard”  $\alpha$ -chymotrypsin but much higher than the “soft” BSA. With  
40  
41 401 the increase of pH, the structural stabilities of both free and surface-bound Cry1Ac decreased.  
42  
43  
44

45 402 Previous studies have reported high conformational stability of Cry1A proteins that retained  
46  
47 403 insecticidal activity on mineral surfaces, as evidenced by the supply rate-independent extent of  
48  
49 404 Cry adsorption on apolar gold or minor molecular-level change of  $\alpha$ -helix and  $\beta$ -sheet contents  
50  
51 405 in surface-bound protein <sup>6, 8, 23</sup>. It was therefore proposed that the small conformational change  
52  
53 406 and associated gain in conformational entropy contributed little to Cry1A adsorption <sup>6, 23</sup>.  
54  
55 407 However, these findings could not explain the rapid and marked decline of protein insecticidal  
56  
57 408 activity in soils <sup>13, 16, 17</sup>. From the perspective of macroscopic-level quantification and DLVO  
58  
59  
60

1  
2  
3 409 prediction, we observed moderate structural loss of adsorbed Cry1Ac with non-DLVO process  
4  
5 410 involved (e.g., entropy gain during protein unfolding), which could be a coherent explanation  
6  
7 411 for the fact that their insecticidal properties remain in soils for only days or weeks<sup>13,16,17</sup>. This  
8  
9 412 can reduce the risk of exposure of non-target soil dwelling organisms, but can also affect the  
10  
11 413 feasibility of monitoring the introduction of Cry toxins to soil by transgenic Bt crops.  
12  
13  
14

#### 15 414 **Declaration of Competing Interest**

16  
17  
18 415 The authors declare that they have no known competing financial interests or personal  
19  
20 416 relationships that could have appeared to influence the work reported in this paper.  
21  
22

#### 23 417 **Acknowledgements**

24  
25  
26 418 This work was supported by the ERASMUS MUNDUS Action 2 PANACEA programme  
27  
28 419 (2012-2647/001-001-EMA2), National Natural Science Foundation of China (31870607), and  
29  
30 420 Youth Innovation Promotion Association of the Chinese Academy of Sciences (2019363). The  
31  
32 421 authors thank Roger Frutos, Cirad, for providing natural strain of *Bacillus thuringiensis*  
33  
34 422 subsp. *Kurstaki* HD73.  
35  
36  
37  
38  
39  
40  
41  
42  
43  
44  
45  
46  
47  
48  
49  
50  
51  
52  
53  
54  
55  
56  
57  
58  
59  
60

1  
2  
3 423 **List of Tables and Figures**  
4  
5

6 424 **Table 1**  
7

8 425 Primary energy barriers ( $1^{\circ}$  max), secondary energy minima ( $2^{\circ}$  min) and corresponding  
9  
10 426 separation distances ( $h$ ) between proteins and montmorillonite calculated by DLVO theory as  
11  
12  
13 427 a function of pH.  
14

15 428 **Table 2**  
16

17  
18 429 Transition enthalpy ( $\Delta H$ ), transition temperature ( $T_m$ ), and full width at half maximum (FWHM)  
19  
20 430 of free and adsorbed Cry1Ac at pH 7.0–9.0. Parameters were obtained from the fitting process  
21  
22 431 in Non-2-State model. Values in parentheses represent standard errors of the fitting parameters  
23  
24  
25 432 given by MicroCal Origin 7.0 software.  
26

27 433 **Table 3**  
28

29  
30 434 Transition enthalpy ( $\Delta H$ ), transition temperature ( $T_m$ ), and full width at half maximum (FWHM)  
31  
32 435 of free and adsorbed chymotrypsin at pH 7.0–9.0. Parameters were obtained from the fitting  
33  
34 436 process in Non-2-State model. Values in parentheses represent standard errors of the fitting  
35  
36  
37 437 parameters given by MicroCal Origin 7.0 software.  
38

39 438 **Table 4**  
40

41  
42 439 Transition enthalpy ( $\Delta H$ ), transition temperature ( $T_m$ ), and full width at half maximum (FWHM)  
43  
44 440 of free and adsorbed BSA at pH 4.0–5.2. Parameters were obtained from the fitting process in  
45  
46 441 Non-2-State model. Values in parentheses represent standard errors of the fitting parameters  
47  
48  
49 442 given by MicroCal Origin 7.0 software.  
50  
51  
52  
53  
54  
55  
56  
57  
58  
59  
60

1  
2  
3 443 **Figure 1.**  
4

5 444 Zeta potentials of Cry1Ac protein, chymotrypsin, bovine serum albumin (BSA), and  
6  
7 445 montmorillonite as a function of pH. Error bars represent the standard deviations of three  
8  
9 446 replicates.  
10  
11  
12

13 447 **Figure 2.**  
14

15 448 Electrostatic energy (a) and DLVO energy profiles (b) of protein-montmorillonite interactions  
16  
17 449 as a function of separation distance ( $h$ ).  $h$  value is scaled by the radius of protein. Mont stands  
18  
19 450 for montmorillonite.  
20  
21

22 451 **Figure 3.**  
23

24 452 DSC thermograms for free and adsorbed (a) Cry1Ac protein, (b) chymotrypsin, and (c) BSA  
25  
26 453 as a function of pH. The up-scan and down-scan rates were 60 °C/h.  
27  
28  
29  
30  
31  
32  
33  
34  
35  
36  
37  
38  
39  
40  
41  
42  
43  
44  
45  
46  
47  
48  
49  
50  
51  
52  
53  
54  
55  
56  
57  
58  
59  
60

1  
2  
3 454 **Supporting Information**  
4  
5

6 455 **Table S1** Experimental conditions of protein adsorption test on montmorillonite (1 mg mL<sup>-1</sup>)  
7  
8  
9 456 and physico-chemical characterization of proteins and montmorillonite. These buffer  
10  
11 457 solutions were used to ensure that the Cry1Ac protein, as well as BSA and chymotrypsin,  
12  
13 458 were always in monomeric forms and carried different surface charges for the  
14  
15 459 comprehensive comparison of their structural stabilities.

16  
17  
18 460 **Table S2** Hydrodynamic diameters of Cry1Ac protein, chymotrypsin, bovine serum albumin  
19  
20 461 (BSA) and montmorillonite as a function of solution pH. The data are presented as the means  
21  
22 462 ± standard deviations.

23  
24  
25 463 **Table S3** Hydrophobicities (%) of Cry1Ac protein, chymotrypsin, bovine serum albumin (BSA)  
26  
27 464 and montmorillonite as a function of solution pH. The data are presented as the means ±  
28  
29 465 standard deviations.

30  
31  
32 466 **Fig. S1** Size distribution of Cry1Ac protein, chymotrypsin, bovine serum albumin (BSA), and  
33  
34 467 montmorillonite measured by dynamic light scattering at 20 °C as a function of pH.

35  
36 468 **Fig. S2** Adsorption percentages of Cry1Ac protein, chymotrypsin, and bovine serum albumin  
37  
38 469 (BSA) on montmorillonite at 20 °C as a function of pH. Error bars represent the standard  
39  
40 470 deviations of three replicates.  
41  
42  
43  
44  
45  
46  
47  
48  
49  
50  
51  
52  
53  
54  
55  
56  
57  
58  
59  
60

471 **Table 1**

472 Primary energy barriers (1° max), secondary energy minima (2° min) and corresponding  
 473 separation distances ( $h$ ) between proteins and montmorillonite calculated by DLVO theory as  
 474 a function of pH.

Protein	pH	1° max ( $k_B T$ )	$h$	2° min ( $k_B T$ )	$h$
Cry1Ac	7.0	0.14	0.23	-0.07	0.80
	8.0	0.38	0.23	-0.05	0.91
	9.0	1.11	0.11	-0.02	1.14
Chymotrypsin	7.0	–	–	–	–
	8.0	–	–	–	–
	9.0	0.52	0.34	–	–
BSA	4.0	–	–	–	–
	4.6	–	–	–	–
	5.2	0.19	0.46	-0.01	2.96

475 Note: “–”denotes no energy barrier or secondary energy minimum.  
 476

477 **Table 2**

478 Transition enthalpy ( $\Delta H$ ), transition temperature ( $T_m$ ), and full width at half maximum (FWHM)  
 479 of free and adsorbed Cry1Ac at pH 7.0–9.0. Parameters were obtained from the fitting process  
 480 in Non-2-State model. Values in parentheses represent standard errors of the fitting parameters  
 481 given by MicroCal Origin 7.0 software.

Cry1Ac state	$T_m$ (°C)	$\Delta H$ (kcal/mol)	FWHM (°C)
Free Cry1Ac (pH 7.0)	76.5 (0.2)	492.0 (16.9)	9.1
Free Cry1Ac (pH 8.0)	73.0 (0.3)	442.5 (15.3)	7.5
Free Cry1Ac (pH 9.0)	70.9 (0.1)	377.4 (12.0)	7.0
Adsorbed Cry1Ac (pH 7.0)	73.2 (0.3)	161.1 (4.1)	9.1
Adsorbed Cry1Ac (pH 8.0)	70.8 (0.1)	143.7 (2.2)	7.8
Adsorbed Cry1Ac (pH 9.0)	69.8 (0.1)	141.4 (2.4)	7.5

482

483 **Table 3**

484 Transition enthalpy ( $\Delta H$ ), transition temperature ( $T_m$ ), and full width at half maximum (FWHM)  
485 of free and adsorbed chymotrypsin at pH 7.0–9.0. Parameters were obtained from the fitting  
486 process in Non-2-State model. Values in parentheses represent standard errors of the fitting  
487 parameters given by MicroCal Origin 7.0 software.

Chymotrypsin state	$T_m$ (°C)	$\Delta H$ (kcal/mol)	FWHM (°C)
Free chymotrypsin (pH 7.0)	47.2 (0.0)	184.7 (1.1)	10.4
Free chymotrypsin (pH 8.0)	43.5 (0.0)	203.1 (0.9)	10.7
Free chymotrypsin (pH 9.0)	42.7 (0.2)	215.2 (6.9)	10.9
Adsorbed chymotrypsin (pH 7.0)	48.4 (0.1)	71.0 (1.0)	10.1
Adsorbed chymotrypsin (pH 8.0)	43.6 (0.3)	85.6 (1.4)	10.7
Adsorbed chymotrypsin (pH 9.0)	42.8 (0.1)	96.6 (1.8)	10.7

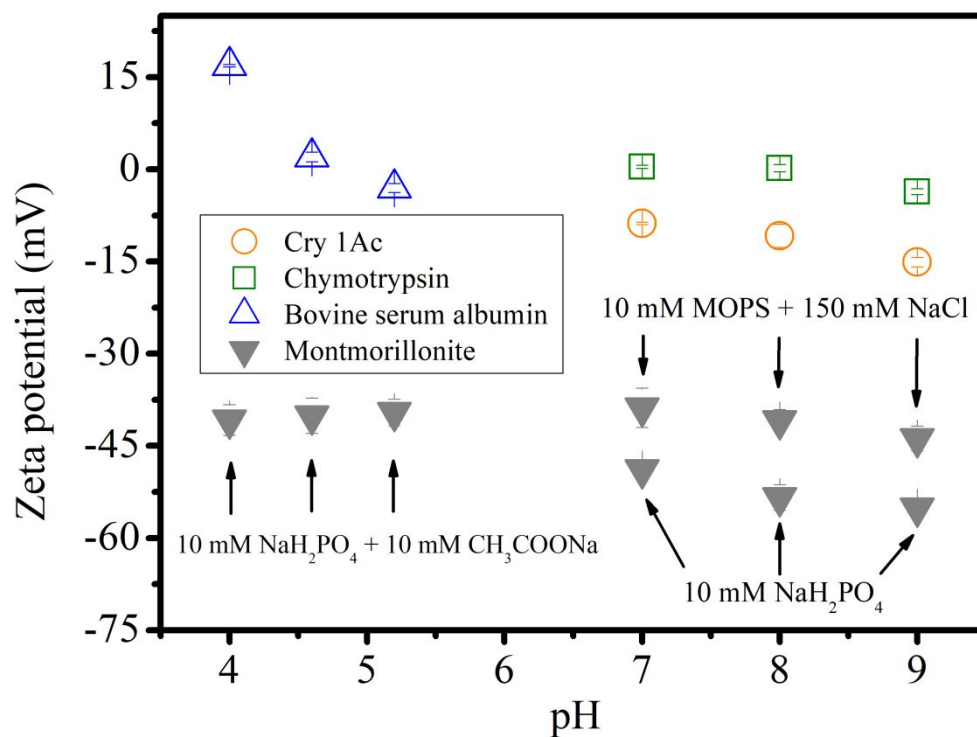
488

489 **Table 4**

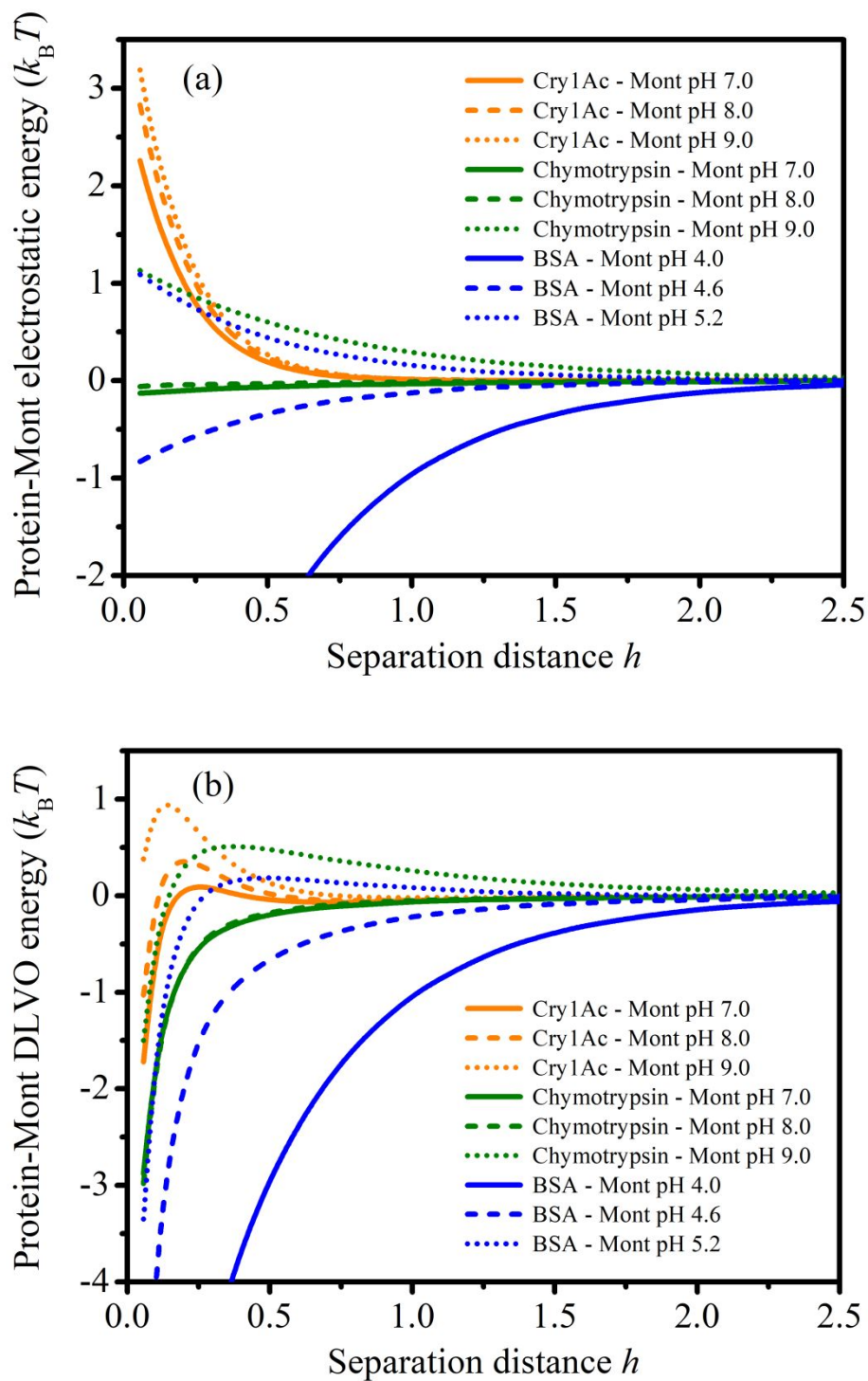
490 Transition enthalpy ( $\Delta H$ ), transition temperature ( $T_m$ ), and full width at half maximum (FWHM)  
 491 of free and adsorbed BSA at pH 4.0–5.2. Parameters were obtained from the fitting process in  
 492 Non-2-State model. Values in parentheses represent standard errors of the fitting parameters  
 493 given by MicroCal Origin 7.0 software.

BSA state	$T_{m1}$ (°C)	$\Delta H_1$ (kcal/mol)	FWHM <sub>1</sub> (°C)	$T_{m2}$ (°C)	$\Delta H_2$ (kcal/mol)	FWHM <sub>2</sub> (°C)
Free BSA (pH 4.0)	44.1 (0.1)	82.0 (1.0)	13.6	67.1 (0.1)	61.3 (0.9)	10.7
Free BSA (pH 4.6)	55.7 (0.1)	121.1 (1.9)	10.7	71.9 (0.1)	87.9 (2.0)	10.1
Free BSA (pH 5.2)	61.8 (0.1)	116.9 (2.3)	9.1	70.5 (0.2)	27.3 (2.5)	7.7
Adsorbed BSA (pH 4.0)	–	–	–	–	–	–
Adsorbed BSA (pH 4.6)	–	–	–	–	–	–
Adsorbed BSA (pH 5.2)	–	–	–	–	–	–

494 Note: The thermograms of adsorbed-state BSA (totally denatured) showed negligible  
 495 calorimetric signals, and no DSC parameters could be obtained by MicroCal Origin 7.0  
 496 software.

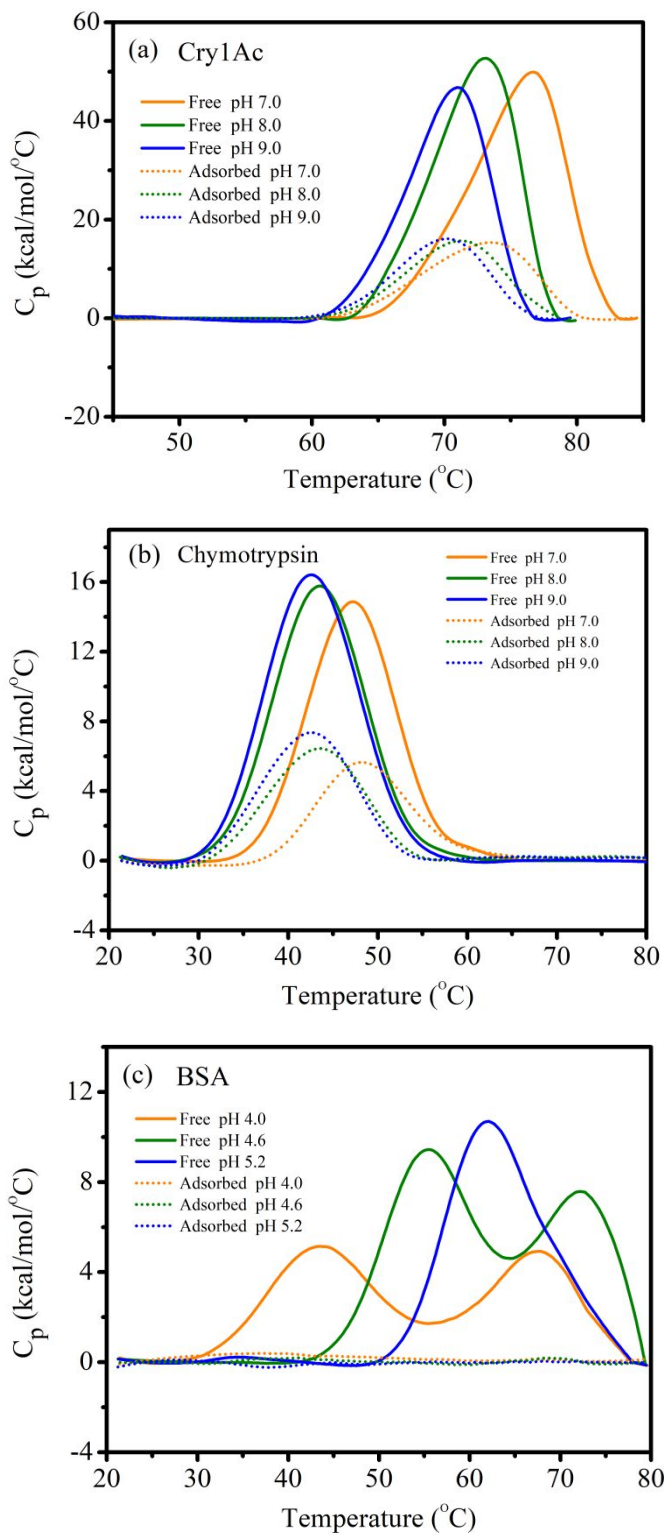
497 **Figures**

498 **Fig. 1.** Zeta potentials of Cry1Ac protein, chymotrypsin, bovine serum albumin (BSA), and  
499 montmorillonite as a function of pH. Error bars represent the standard deviations of three  
500 replicates.  
501



502

503 **Fig. 2.** (a) Electrostatic energy and (b) DLVO energy profiles of protein-montmorillonite  
 504 interactions as a function of separation distance ( $h$ ).  $h$  value is scaled by the radius of protein.  
 505  
 506 Mont stands for montmorillonite.



507

508

509

510 **Fig. 3.** DSC thermograms for free and adsorbed (a) Cry1Ac protein, (b) chymotrypsin, and (c)

511 BSA as a function of pH. The up-scan and down-scan rates were 60 °C/h.

## References

1. Li, Z. L.; Cui, J.; Mi, Z. R.; Tian, D. S.; Wang, J. S.; Ma, Z. L.; Wang, B. X.; Chen, H. Y. H.; Niu, S. L., Responses of soil enzymatic activities to transgenic *Bacillus thuringiensis* (Bt) crops-A global meta-analysis. *Science of the Total Environment* **2019**, 1830-1838.
2. Brookes, G.; Barfoot, P., Environmental impacts of genetically modified (GM) crop use 1996-2018: impacts on pesticide use and carbon emissions. *GM Crops & Food* **2020**, *11* 215-241.
3. James, C., *Global status of commercialized biotech/GMCrops*. Ithaca, NY, 2017.
4. Miethling-Graff, R.; Dockhorn, S.; Tebbe, C. C., Release of the recombinant Cry3Bb1 protein of Bt maize MON88017 into field soil and detection of effects on the diversity of rhizosphere bacteria. *European Journal of Soil Biology* **2010**, *46*, 41-48.
5. Zhang, M.; Feng, M.; Xiao, L.; Song, X. Y.; Yang, W. D.; Ding, G. W., Impact of water content and temperature on the degradation of Cry1Ac protein in leaves and buds of Bt cotton in the soil. *PLoS One* **2015**, *10* e115240.
6. Sander, M.; Madliger, M.; Schwarzenbach, R. P., Adsorption of transgenic insecticidal Cry1Ab protein to SiO<sub>2</sub>. I. Forces driving adsorption. *Environmental Science and Technology* **2010**, *44*, 8870-8876.
7. Helassa, N.; Quiquampoix, H.; Noinville, S.; Szponarski, W.; Staunton, S., Adsorption and desorption of monomeric Bt (*Bacillus thuringiensis*) Cry1Aa toxin on montmorillonite and kaolinite. *Soil Biology and Biochemistry* **2009**, *41*, 498-504.
8. Helassa, N.; Revault, M.; Quiquampoix, H.; Dejardin, P.; Staunton, S.; Noinville, S., Adsorption on montmorillonite prevents oligomerization of Bt Cry1Aa toxin. In *Science*, J. o. C. a. I., Ed. United States, 2011; Vol. 356, pp 718-25.
9. Janot, J. M.; Boissiere, M.; Thami, T.; Tronel-Peyroz, E.; Helassa, N.; Noinville, S.; Quiquampoix, H.; Staunton, S.; Dejardin, P., Adsorption of Alexa-Labeled Bt Toxin on Mica, Glass, and Hydrophobized Glass: Study by Normal Scanning Confocal Fluorescence. *Biomacromolecules* **2010**, *11*, 1661-1666.
10. Georgsson, G.; Sigurdarson, S.; Brown, P., Infectious agent of sheep scrapie may persist in the environment for at least 16 years. *Journal of General Virology* **2006**, *87*, (Pt 12), 3737-3740.
11. Seidel, B.; Thomzig, A.; Buschmann, A.; Groschup, M. H.; Peters, R.; Beekes, M.; Terytze, K., Scrapie Agent (Strain 263K) can transmit disease via the oral route after persistence in soil over years. In *One*, P., Ed. 2007; Vol. 2, p e435.
12. Sims, S. R.; Holdens, L. R., Insect bioassay for determining soil degradation of *Bacillus thuringiensis* subsp. *Kurstaki* Cry1A(b) protein in corn tissue. *Environmental Entomology* **1996**, *25* 659-664.
13. Herman, R. A.; Wolt, J. D.; Halliday, W. R., Rapid degradation of the Cry1F insecticidal crystal protein in soil. *Journal of Agricultural and Food Chemistry* **2002**, *50* 7076-7078, .
14. Wang, H.; Ye, Q.; Wang, W.; Wu, L.; Wu, W., Cry1Ab protein from Bt transgenic rice does not residue in rhizosphere soil. *Environmental Pollution* **2006**, *143*, 449-55.
15. Helassa, N.; M'Charek, A.; Quiquampoix, H.; Noinville, S.; Déjardin, P.; Frutos, R.; Staunton, S., Effects of physicochemical interactions and microbial activity on the persistence of Cry1Aa Bt (*Bacillus thuringiensis*) toxin in soil. *Soil Biology and Biochemistry* **2011**, *43*, (5), 1089-1097.
16. Hung, T. P.; Truong, L. V.; Binh, N. D.; Frutos, R.; Quiquampoix, H.; Staunton, S., Persistence of detectable insecticidal proteins from *Bacillus thuringiensis* (Cry) and toxicity after adsorption on contrasting soils. *Environmental Pollution* **2016**, *208*, (Pt B), 318-25.
17. Liu, J.; Liang, Y.; Hu, T.; Zeng, H.; Gao, R.; Wang, L.; Xiao, Y., Environmental fate of Bt proteins in soil: Transport, adsorption/desorption and degradation. *Ecotoxicology and Environmental Safety* **2021**, *226* 112805.
18. Stotzky, G., Persistence and biological activity in soil of the insecticidal proteins from *Bacillus thuringiensis*, especially from transgenic plants. *Plant and Soil* **2005**, *266*, 77-89.
19. Muchaonyerwa, P.; Chevallier, T.; Pantani, O. L.; Nyamugafata, P.; Mpeperekwi, S.; Chenu, C., Adsorption of the pesticidal toxin from *Bacillus thuringiensis* subsp. *tenebrionis* on tropical soils and their particle-size fractions. *Geoderma* **2006**, *133*, 244-257.
20. Feng, Y.; Ling, L.; Fan, H. Z.; Liu, Y. H.; Tan, F. X.; Shu, Y. H.; Wang, J. W., Effects of temperature, water content and pH on degradation of Cry1Ab protein released from Bt corn straw in soil. *Soil Biology and Biochemistry* **2011**, *43*, 1600-1606.
21. Clark, B. W.; Phillips, T. A.; Coats, J. R., Environmental fate and effects of *Bacillus thuringiensis* (Bt) proteins from transgenic crops: a review. *Journal of Agricultural and Food Chemistry* **2005**.
22. Aronson, A. I.; Shai, Y., Why *Bacillus thuringiensis* insecticidal toxins are so effective: unique features of their mode of action. *FEMS Microbiology Letters* **2001**, *195*, 1-8.
23. Madliger, M.; Gasser, C. A.; Schwarzenbach, R. P.; Sander, M., Adsorption of transgenic insecticidal Cry1Ab protein to silica particles, Effects on transport and bioactivity. *Environmental Science and Technology* **2011**, *45* 4377-4384.
24. Brandes, N.; Welzel, P. B.; Werner, C.; Kroh, L. W., Adsorption-induced conformational changes of

- 1  
2  
3 572 proteins onto ceramic particles: Differential scanning calorimetry and FTIR analysis. *Journal of Colloid and*  
4 573 *Interface Science* **2006**, *299*, 56-69.
- 5 574 25. Jeyachandran, Y.; Mielczarski, E.; Rai, B.; Mielczarski, J., Quantitative and qualitative evaluation of  
6 575 adsorption/desorption of bovine serum albumin on hydrophilic and hydrophobic surfaces. *Langmuir* **2009**, *25*,  
7 576 11614-11620.
- 8 577 26. Kubiak-Ossowska, K.; Jachimska, B.; Mulheran, P. A., How negatively charged proteins adsorb to  
9 578 negatively charged surfaces: a molecular dynamics study of BSA adsorption on silica. *Journal of Physical*  
10 579 *Chemistry B* **2016**, *120* 10463-10468.
- 11 580 27. Dalkas, G.; Euston, S. R., Molecular simulation of protein adsorption and conformation at gas-liquid,  
12 581 liquid-liquid and solid-liquid interfaces. *Current Opinion in Colloid and Interface Science* **2019**, *41* 1-10.
- 13 582 28. Jachimska, B.; Tokarczyk, K.; Lapczyńska, M., Structure of bovine serum albumin adsorbed on silica  
14 583 investigated by quartz crystal microbalance. *Colloids and Surfaces A* **2016**, *489*, 163-172.
- 15 584 29. Quiquampoix, H.; Burns, R. G., Interactions between proteins and soil mineral surfaces: environmental  
16 585 and health consequences. *Elements* **2007**, *3* 401-406.
- 17 586 30. Quiquampoix, H., Enzymes and Proteins, Interactions with soil-constituent surfaces. In *In: Encyclopedia*  
18 587 *of Soil Science (Ed. W. Chesworth)*. Springer, 2008; pp 210-216.
- 19 588 31. Lousinian, S.; Missopolinou, D.; Panayiotou, C., Fibrinogen adsorption on zinc oxide nanoparticles: A  
20 589 Micro-Differential Scanning Calorimetry analysis. *Journal of Colloid and Interface Science* **2013**, *395* 294-299.
- 21 590 32. Wen, J.; Arthur, J.; Chemmalil, L.; Muzammil, S.; Gabrielson, J.; Jiang, Y. J., Applications of Differential  
22 591 Scanning Calorimetry for Thermal Stability Analysis of Proteins: Qualification of DSC. *Journal of*  
23 592 *Pharmaceutical Sciences* **2012**, *101*, 955-964.
- 24 593 33. Amani, M.; Moosavi-Movahedi, A. A.; Kurganov, B. I., What can we get from varying scan rate in protein  
25 594 differential scanning calorimetry? *International Journal of Biological Macromolecules* **2017**, *99*, 151-159.
- 26 595 34. Madliger, M.; Sander, M.; Schwarzenbach, R. P., Adsorption of transgenic insecticidal Cry1Ab protein  
27 596 to SiO<sub>2</sub>: 2. Patch-controlled electrostatic attraction. *Environmental Science and Technology* **2010**, *44*, 8877-8883.
- 28 597 35. Sander, M.; Tomaszewski, J. E.; Madliger, M.; Schwarzenbach, R. P., Adsorption of insecticidal Cry1Ab  
29 598 protein to humic substances. 1. Experimental approach and mechanistic aspects. *Environmental Science and*  
30 599 *Technology* **2012**, *46* 9923-9931.
- 31 600 36. Miao, S.; Yuan, X.; Liang, Y.; Wang, H.; Leng, L.; Wu, Z.; Jiang, L.; Li, Y.; Mo, D.; Zeng, G., In situ  
32 601 surface transfer process of Cry1Ac protein on SiO<sub>2</sub>: The effect of biosurfactants for desorption. *Journal of*  
33 602 *Hazardous Materials* **2018**, *341* 150-158.
- 34 603 37. Derjaguin, B.; Landau, L., Theory of the stability of strongly charged lyophobic sol and of the adhesion  
35 604 of strongly charged particles in solutions of electrolytes. *Acta Physicochimica U.R.S.S.* **1941**, *14*, 633-662.
- 36 605 38. Verwey, E.; Overbeek, J., *Theory of the Stability of Lyophobic Colloids*. Netherlands: Elsevier Publishing  
37 606 Company, Inc., Amsterdam, 1948.
- 38 607 39. Farrell, M.; Beaudoin, S., Surface forces and protein adsorption on dextran- and polyethylene glycol-  
39 608 modified polydimethylsiloxane. *Colloids and Surfaces B* **2010**, *81*, 468-475.
- 40 609 40. Haynes, C. A.; Norde, W., Globular proteins at solid/liquid interfaces. *Colloids and Surfaces A* **1994**, *2*,  
41 610 517-566.
- 42 611 41. Coglitore, D.; Janot, J. M.; Balme, S., Protein at liquid solid interfaces: Toward a new paradigm to change  
43 612 the approach to change the approach to design hybrid/solid-state materials. *Advances in Colloid and Interface*  
44 613 *Science* **2019**, *270*, 278-290.
- 45 614 42. Fu, Q.; Dong, Y.; Hu, H.; Huang, Q., Adsorption of the insecticidal protein of *Bacillus thuringiensis* subsp.  
46 615 *kurstaki* by soil minerals: Effects of organic acid ligands. *Applied Clay Science* **2007**, *37*, (1-2), 201-206.
- 47 616 43. Fu, Q.; Y., P.; Huang, T.; Hu, H.; Deng, Y.; Yu, X., Effects of ionic strength and sesquioxides on  
48 617 adsorption of toxin of *Bacillus thuringiensis* subsp. *kurstaki* on soils. *Pedosphere* **2012**, *22*, 96-102.
- 49 618 44. Tabashnik, B. E.; Brévault, T.; Carrière, Y., Insect resistance to Bt crops: lessons from the first billion  
50 619 acres. *Nature Biotechnology* **2013**, *31*, 510-521.
- 51 620 45. Hopkins, D. W.; Gregorich, E. G., Detection and decay of the Bt endotoxin in soil from a field trial with  
52 621 genetically modified maize. *European Journal of Soil Science* **2003**, *54*, 793-800.
- 53 622 46. Gruber, H.; V., P.; Meyer, H. H. D.; Muller, M., Determination of insecticidal Cry1Ab protein in soil  
54 623 collected in the final growing seasons of a nine-year field trial of Bt-maize MON810. *Transgenic Research* **2012**,  
55 624 *21* 77-88.
- 56 625 47. Powers, E. T.; Powers, D. L., The kinetics of nucleated polymerizations at high concentrations: Amyloid  
57 626 fibril formation near and above the "supercritical concentration". *Biophysical Journal* **2006**, *91* 122-132.
- 58 627 48. Welzel, P. B., Investigation of adsorption-induced structural changes of proteins at solid/liquid interfaces  
59 628 by differential scanning calorimetry. *Thermochimica Acta* **2002**, 175-188.
- 60 629 49. Servagent-Noinville, S.; Revault, M.; Quiquampoix, H.; Baron, M. H., Conformational changes of bovine  
61 630 serum albumin induced by adsorption on different clay surfaces: FTIR analysis. *Journal of Colloid and Interface*  
62 631 *Science* **2000**, *221* 273-283.

1  
2  
3  
4  
5  
6  
7  
8  
9  
10  
11  
12  
13  
14  
15  
16  
17  
18  
19  
20  
21  
22  
23  
24  
25  
26  
27  
28  
29  
30  
31  
32  
33  
34  
35  
36  
37  
38  
39  
40  
41  
42  
43  
44  
45  
46  
47  
48  
49  
50  
51  
52  
53  
54  
55  
56  
57  
58  
59  
60  
61

50. Xiong, K.; Fan, Q.; Wu, T.; Shi, H.; Chen, L.; Yan, M., Enhanced bovine serum albumin adsorption on the N-hydroxysuccinimide activated graphene oxide and its corresponding cell affinity. *Material Science and Engineering C* **2017**, *81*, 386–392.
51. Hildebrand, N.; Köppen, S.; Derr, L.; Li, K.; Koleini, M.; Rezwan, K.; Colombi Ciacchi, L., Adsorption orientation and binding motifs of lysozyme and chymotrypsin on amorphous silica. *Journal of Physical Chemistry C* **2015**, *119*, 7295–7307.
52. Derr, L.; Dringen, R.; Treccani, L.; Hildebrand, N.; Ciacchi, L. C.; Rezwan, K., Physisorption of enzymatically active chymotrypsin on titania colloidal particles. *Journal of Colloid Interface Science* **2015**, *455*, 236–244.
53. Helassa, N.; Daudin, G.; Noinville, S.; Janot, J.-M.; Déjardin, P.; Staunton, S.; Quiquampoix, H., Mobility of adsorbed Cry1Aa insecticidal toxin from *Bacillus thuringiensis* (Bt) on montmorillonite measured by fluorescence recovery after photobleaching (FRAP). *Philosophical Magazine* **2010**, *90*, (17-18), 2365-2371.
54. Mooney, R. W.; Keenan, A. G.; Wood, L. A., Adsorption of water vapor by montmorillonite. I. Heat of desorption and application of BET theory. *Journal of the American Chemistry Society* **1952**, *74*, 1367–1371.
55. Quiquampoix, H., A stepwise approach to the understanding of extracellular enzyme activity in soil I. Effect of electrostatic interactions on the conformation of a  $\beta$ -D-glucosidase adsorbed on different mineral surfaces. *Biochimie* **1987**, *69*, 753–763.
56. Lahari, C.; Jasti, L. S.; Fadnavis, N. W.; Sontakke, K.; Ingavle, G.; Deokar, S.; Ponrathnam, S., Adsorption induced enzyme denaturation: the role of polymer hydrophobicity in adsorption and denaturation of  $\alpha$ -chymotrypsin on allyl glycidyl ether (AGE)-ethylene glycol dimethacrylate (EGDM) copolymers. *Langmuir* **2010**, *26* 1096-1106.
57. Tazehkand, S. S.; Torkzaban, S.; Bradford, S. A.; Walker, S. L., Cell preparation methods influence *Escherichia coli* D21g surface chemistry and transport in saturated sand. *Journal of Environmental Quality* **2008**, *37*, 2108-2115.
58. Martin, A. H.; Meinders, M. B.; Bos, M. A.; Cohen Stuart, M. A.; van Vliet, T., Conformational aspects of proteins at the air/water interface studied by infrared reflection-absorption spectroscopy. *Langmuir* **2003**, *19* 2922-2928.
59. Togashi, D. M.; Ryder, A. G.; Heiss, G., Quantifying adsorbed protein on surfaces using confocal fluorescence microscopy. *Colloids and Surfaces B* **2009**, *72* 219-229.
60. Gray, J. J., The interaction of proteins with solid surfaces. *Current Opinion in Structural Biology* **2004**, *14* 110-115.
61. Kim, J.; Desch, R. J.; Thiel, S. W.; Gulians, V. V.; Pinto, N. G., Energetics of lysozyme adsorption on mesostructured cellular foam silica: Effect of salt concentration. *Journal of Chromatography A* **2011**, *1218* 6697-6704.
62. Vigeant, M.; Ford, R. M., Interactions between motile *Escherichia coli* and glass in media with various ionic strengths, as observed with a three-dimensional-tracking microscope. *Applied and Environmental Microbiology* **1997**, *63* 3474-3479.
63. Oberholzer, M. R.; Wagner, N. J.; Lenhoff, A. M., Grand canonical Brownian dynamics simulation of colloidal adsorption. *Journal of Chemical Physics* **1997**, *107*, 9157-9167.
64. Miyahara, M.; Watanabe, S.; Gotoh, Y.; Higashitani, K., Adsorption and order formation of colloidal nanoparticles on a substrate: a Brownian dynamics study. *Journal of Chemical Physics* **2004**, *120* 1524-1534.
65. Thrash Jr, M. E.; Pinto, N. G., Incorporating water-release and lateral protein interactions in modeling equilibrium adsorption for ion-exchange chromatography. *Journal of Chromatography A* **2006**, *1126* 304-310.
66. Michnik, A.; Michalik, K.; Kluczevska, A.; Drzazga, Z., Comparative DSC study of human and bovine serum albumin. *Journal of Thermal Analysis and Calorimetry* **2006**, *84*, 113-117.
67. Larsericsdotter, H.; Oscarsson, S.; Buijs, J., Structure, stability, and orientation of BSA adsorbed to silica. *Journal of Colloid and Interface Science* **2005**, *289* 26-35.
68. Rabe, M.; Verdes, D.; Seeger, S., Understanding protein adsorption phenomena at solid surfaces. *Advances in Colloid and Interface Science* **2011**, *162* 87-106.
69. Aschi, A.; Mbarek, M.; Othman, M.; Gharbi, A., Study of thermally and chemically unfolded conformations of bovine serum albumin by means of dynamic light scattering. *Materials Science and Engineering C-Biomimetic and Supramolecular Systems* **2008**, *28* 594-600.
70. Hanlon, A. D.; Larkin, M. I.; Reddick, R. M., Free-solution, label-free protein-protein interactions characterized by dynamic light scattering. *Biophysical Journal* **2010**, *98* 297-304.
71. Masson, L.; Mazza, A.; Sangadala, S.; Adang, M. J.; Brousseau, R., Polydispersity of *Bacillus thuringiensis* Cry1 toxins in solution and its effect on receptor binding kinetics. *Biochimical et Biophysical Acta-Protein Structure and Molecular Enzymology* **2002**, *1594* 266-275.
72. Kubiak-Ossowska, K.; Jachimaska, B.; Qaraghuli, M. A.; Mulheran, P. A., Protein interactions with negatively charged inorganic surfaces. *Current Opinion in Colloid and Interface Science* **2019**, *41* 104-117.
73. Boubeta, F. M.; Soler-Illia, G. J. A. A.; Tagliacruzchi, M., Electrostatically driven protein adsorption-

- charge patches versus charge regulation. *Langmuir* **2018**, *34* 15727-15738.
74. Dammak, M.; Ali, M. B.; Jaoua, S.; Tounsi, S., Amino acids Y229 and F603 are involved in *Bacillus thuringiensis* Cry1Ac d-endotoxin stability and toxicity. *FEMS Microbiology Letters* **2012**, *329*, 54–60.
75. Lee, M. K.; You, T. H.; Gould, F. L.; Dean, D. H., Identification of residues in domain III of *Bacillus thuringiensis* Cry1Ac toxin that affect binding and toxicity. *Applied and Environmental Microbiology* **1999**, *65*, 4513–4520.
76. Quiquampoix, H.; Ratcliffe, R. G., A <sup>31</sup>P NMR study of the adsorption of bovine serum albumin on montmorillonite using phosphate and the paramagnetic cation Mn<sup>2+</sup>: modification of conformation with pH. *Journal of Colloid and Interface Science* **1992**, *148* 343-352.
77. Precupas, A.; Gheorghe, D.; Botea-Petcu, A.; Leonties, A. R.; Sandu, R.; Popa, V. T.; Mariussen, E.; Naouale, E.; Runden-Pran, E.; Dumit, V.; Xue, Y.; Cimpan, M. R.; Dusinska, M.; Haase, A.; Tanasescu, S., Thermodynamic parameters at bio-nano interface and nanomaterial toxicity: A case study on BSA interaction with ZnO, SiO<sub>2</sub> and TiO<sub>2</sub>. *Chemical Research in Toxicology* **2020**, *33* 2054-2071.
78. Norde, W.; Giacomelli, C. E., BSA structural changes during homomolecular exchange between the adsorbed and the dissolved states. *Journal of Biotechnology* **2000**, *79*, 259-268.
79. Banigan, J. R.; Leninger, M.; Her, A. S.; Traaseth, N. J., Assessing interactions between a polytopic membrane protein and lipid bilayers using differential scanning calorimetry and solid-state NMR. *Journal of Physical Chemistry B* **2018**, *122* 2314-2322.
80. Grochulski, P.; Masson, L.; Borisova, S.; Pusztai-Carey, M.; Schwartz, J. L.; Brousseau, R.; Cygler, M., *Bacillus thuringiensis* Cry1A(a) insecticidal toxin: crystal structure and channel formation. *Journal of Molecular Biology* **1995**, *254*, 447–464.
81. Soberón, M.; Monnerat, R.; Bravo, A., Mode of action of Cry toxins from *Bacillus thuringiensis* and resistance mechanisms. *Microbial Toxins* **2018**, 1-28.
82. Gao, H.; Geng, X. P.; Wang, B. H.; Zhou, Y., Studies on the conformational change of adsorbed BSA onto a moderately hydrophobic surface at different denaturant concentrations and surface coverages. *Journal of Colloid and Interface Science* **2010**, *344* 468-474.
83. Baron, M. H.; Revault, M.; Servagent-Noinville, S.; Abadie, J.; Quiquampoix, H., Chymotrypsin adsorption on montmorillonite: enzymatic activity and kinetic FTIR structural analysis. *Journal of Colloid and Interface Science* **1999**, *214* 319-332.
84. Larsericsdotter, H.; Oscarsson, S.; Buijs, J., Thermodynamic analysis of proteins adsorbed on silica particles: electrostatic effects. *Journal of Colloid and Interface Science* **2001**, *237* 98-103.
85. Chen, G.; Walker, S. L., Role of solution chemistry and ion valence on the adhesion kinetics of groundwater and marine bacteria. *Langmuir* **2007**, *23* 7162-7169.
86. Giacomelli, C. E.; Norde, W., The adsorption-desorption cycle. Reversibility of the BSA-silica system. *Journal of Colloid and Interface Science* **2001**, *233* 234-240.
87. Arai, T.; Norde, W., The Behavior of Some Model Proteins at Solid-Liquid Interfaces 1. Adsorption from Single Protein Solutions. *Colloids and Surfaces A* **1990**, *51*, 1–15.
88. Norde, W.; MacRitchie, F.; Nowicka, G.; Lyklema, J., Protein Adsorption at Solid-Liquid Interfaces: Reversibility and Conformation Aspects. *Journal of Colloid and Interface Science* **1986**, *112*, 447–456.
89. Koo, J.; Erlkamp, M.; Grobelny, S.; Steitz, R.; Czeslik, C., Pressure-Induced Protein Adsorption at Aqueous-Solid Interfaces. *Langmuir* **2013**, *29*, 8025–8030.
90. Vijayakumar, S.; Vishveshwara, S.; Ravishanker, G.; Beveridge, D. L., Differential Stability of Beta-Sheets and Alpha-Helices in Beta- Lactamase: A High Temperature Molecular Dynamics Study of Unfolding Intermediates *Biophysical Journal* **1993**, *65*, 2304–2312.
91. Uniprot, <https://www.uniprot.org/uniprot/P02769>.
92. Uniprot, <https://www.uniprot.org/uniprot/P05068>.
93. Uniprot, <https://www.uniprot.org/uniprot/P00766>.

739